The potential of Tidal River Management for flood alleviation in South Western Bangladesh

Mohammed Sarfaraz Gani Adnan [a,c*], Rocky Talchabhadel [b], Hajime Nakagawa [b], Jim W. Hall [a]

[a] Environmental Change Institute, School of Geography and the Environment, University of Oxford, South Parks Road, OX13QY Oxford, United Kingdom

[b] Disaster Prevention Research Institute, Kyoto University, Japan

[c] Department of Urban and Regional Planning, Chittagong University of Engineering and Technology (CUET), Chittagong 4349, Bangladesh

Abstract

Reduced sediment deposition, land subsidence, channel siltation, and salinity intrusion has been an unintended consequence of the construction of polders in the south western delta of Bangladesh in the 1960s. Tidal River Management (TRM) is a process that is intended to temporarily reverse these processes and restore sediment deposition and land elevation at the low-lying sites, known as 'beels', where TRM is carried out. However, there is limited evidence to prioritise sites for TRM on the basis of its potential effectiveness at alleviating flooding. In this study, the south western delta of Bangladesh was classified according to different flood susceptible zones. In south western Bangladesh, the major portion of agricultural and aquaculture land is located within flood susceptible zones (65% and 81%, respectively). 44.5% of the total population in embanked regions live in areas classified as being flood susceptible. This study identified 106 'beels' suitable for TRM. Modelling of potential sediment deposition predicted that the consequent increase in land elevation could be up to 1.4m in five years, which would alleviate land subsidence and modify several geomorphological factors such as aspect, slope, curvature, and Stream Power Index (SPI). Implementation of TRM at these sites could potentially reduce the probability of annual flooding from 0.86 (on average) to 0.57 (on average). Therefore, TRM could lower the flood susceptible area by 35% in suitable 'beels'. Whilst during the implementation of TRM agriculture has to cease for a few years, a systematic programme of TRM could result in a long-term increase in agricultural production by reducing flood susceptibility of agricultural lands in delta regions.

Key words: Tidal River Management; flood susceptibility; frequency ratio; logistic regression; sediment transportation; Bangladesh coastal region

1. Introduction

Pluvial flooding during the monsoon period affects the south western coastal region of Bangladesh annually (Warner et al., 2018), inundating agricultural lands and damaging people's livelihoods (Alam et al., 2017; Awal, 2014). This form of flood occurs either due to a short term intense or prolonged low to moderate level precipitation (Falconer et al., 2009). Pluvial flooding has become much more severe in this region because of land subsidence, siltation in riverbeds restricting drainage, and land use change e.g., the encroachment of drainage channels (Alam et al., 2017).

Following a major cyclone and storm surge flood in 1953, the East Pakistan Water and Power Development Authority (now the Bangladesh Water Development Board (BWDB)) invested in a major Coastal Embankment Project (CEP). Since 1960, a total of 139 polders (enclosed coastal embankments) were constructed throughout the coastal region, with the stated objective of preventing inundation by saline water of agricultural lands during surge tides and cyclones, increasing agricultural production and ensuring food security (Islam et al., 2016; Warner et al., 2018). The construction of polders resulted in increased agricultural production until the 1980s (Nowreen et al., 2014). On the other hand, the polder system disconnected the delta floodplain from the river channel network, which had the consequences of promoting land subsidence in the embanked areas (Alam et al., 2017; Auerbach et al., 2015; Van Staveren et al., 2017). The embanked region in the south western coast of Bangladesh has lost 1.0-1.5m of land elevation since the construction of the polders (Auerbach et al., 2015). The polder system restricted silts from rivers being deposited onto 'beels' (a local term referring to surface depression), whilst accelerating sedimentation in riverbeds and increasing river water levels. In turn, this prevents gravity drainage systems within the embanked region from functioning properly (Mutahara et al., 2018). As a result, runoff generated from monsoon precipitation accumulates in and floods, polders (Auerbach et al., 2015; Choudhury et al., 2004; Talchabhadel et al., 2018). Projected sea level rise (IPCC, 1996) will increase the tidal water level within the adjacent Bay of Bengal, worsening drainage congestion and pluvial flooding in polders (Awal, 2014). Pluvial floods lead to economic losses either by damaging crops or delaying cultivation of winter crops (*Boro* rice), affecting the livelihood of millions of people across the Ganges-Brahmaputra-Meghna (GBM) delta, and particularly poor and marginal farmers living inside polders (Alam et al., 2017). For instance, a pluvial flood in 2011 inundated more than 128,000ha of croplands for 90 days in three south western coastal districts of Bangladesh: Khulna, Satkhira, and Jessore (Awal, 2014).

Tidal River Management (TRM) has been adopted in an attempt to address the worsening impacts of pluvial flooding, salinity, and siltation in riverbeds, by restoring sedimentation in low-lying 'beels'. The idea of TRM is to bring sediment-carrying tidal water into selected 'beels' two times a day through a controlled breaching in polders, to allow sedimentation and elevate the land (Amir and Khan, 2019; Gain et al., 2017; Masud et al., 2018; Seijger et al., 2019; Talchabhadel et al., 2018). Although

historically a community-driven approach, the BWDB has been responsible for implementing TRM since 1997. From 1991 to 2013, TRM has been implemented (either by local people or the BWDB) in 12 out of 35 designated 'beels' in the south western coastal zone (Gain et al., 2017; Masud et al., 2018). Implementation of TRM in the south western embanked region is still an ongoing process (Gain et al., 2017). However, governance issues (e.g. disagreement about TRM sites and issues with compensation) were reported during the implementation and operation of TRM projects (Gain et al., 2017; Mutahara et al., 2018). Since TRM makes the 'beel' unsuitable for crop production during the implementation period (Masud et al., 2018), an explicit engagement of different stakeholders (landowners and agricultural workers who are fully or partially dependent on the land in TRM sites) is required from project planning to implementation phases (Mutahara et al., 2018).

Existing studies have described both positive and negative impacts of TRM projects on local communities and the environment (Amir and Khan, 2019; Gain et al., 2017; Masud et al., 2018; Mutahara et al., 2018). For instance, the operation of TRM in 'beel' Bhaina (1997-2001) led to a raise in land elevation by 1m on average and consequently increased the depth and width of the adjacent Hari River by 10-12m and 2-3 times, respectively (Gain et al., 2017; Mutahara et al., 2018). On the other hand, an unplanned TRM operation could lead to riverbank erosion, salinity intrusion, and inundation in built-up areas (Gain et al., 2017; Talchabhadel et al., 2018). For instance, in 'beel' Khuksia, an unplanned implementation of TRM, without sufficient cooperation between stakeholders and government agencies, resulted in several disruptions during implementation (2006-2012). Thus, inundation problems remained after the implementation of TRM in Khukshia (Figure 1 (c)) because of an uneven land elevation caused by an uneven distribution of deposited sediments (Gain et al., 2017). Also, various environmental and economic issues can arise during the implementation of TRM (Masud et al., 2018). These issues include an increase in salinity intrusion, inundation of agricultural lands, riverbank erosion, and disruption of transport services (Gain et al., 2017).

Evaluating the impact of TRM on flooding is a complex process because (1) the rate of sedimentation vary spatially and temporally (Gain et al., 2017) and (2) flooding is an outcome of various combinations of geomorphological, hydrological, and anthropogenic processes (Khosravi et al., 2016; Pradhan et al., 2010; Tehrany et al., 2014a). Although some benefits of TRM have been reported in the literature (Amir and Khan, 2019; Gain et al., 2017), there remains a lack of evidence of how the implementation of TRM will change the actual mechanism of flooding, leading to a potential change in the extent of the flood susceptible area in embanked regions. Care should be given to identify areas suitable for operating TRM to avoid adverse impacts on society and the environment. To address these challenges, (1) flood mechanisms in the south western embanked region of Bangladesh were analysed, estimating the influence of various flood causative factors on flood susceptibility, and (2) the impact of TRM on flood susceptibility was quantified, modelling sediment transportation and deposition in suitable TRM sites

comparing flood susceptibility before and after TRM implementation, in order to prioritise suitable sites.

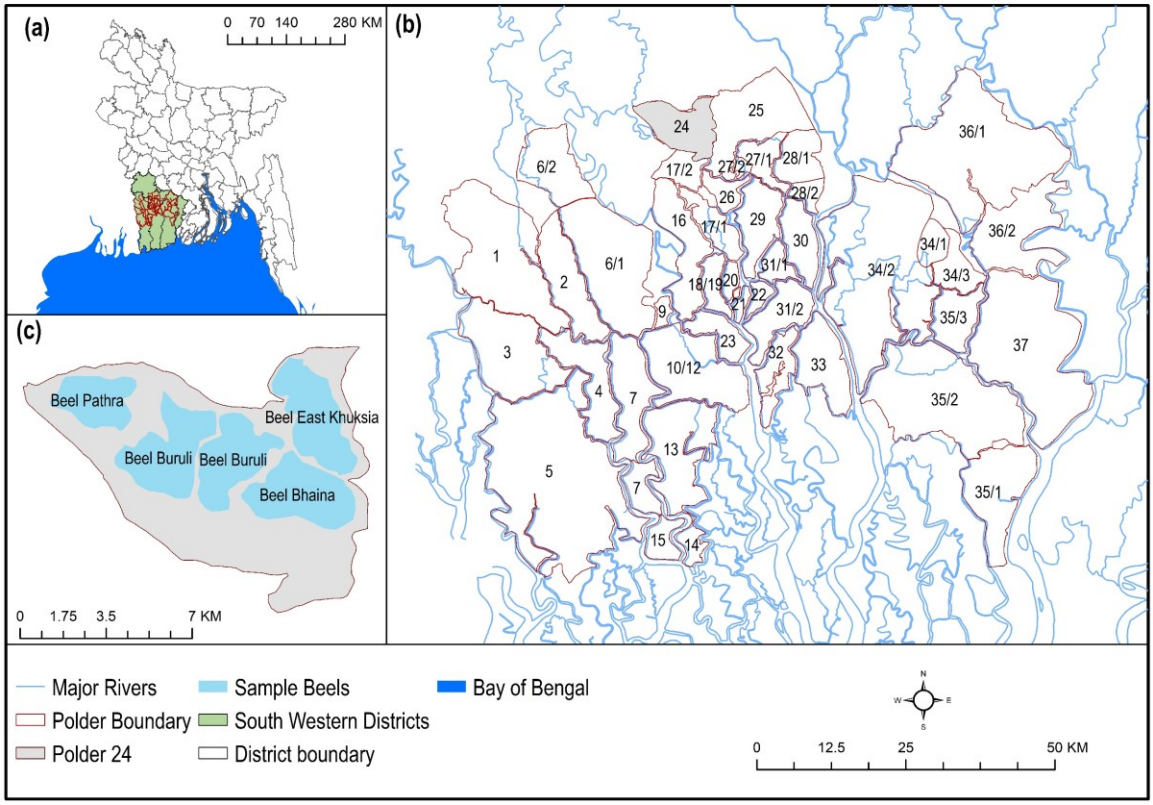

Figure 1: Study area map

2. Materials and methods

This study was conducted in two stages. First, the influence of various factors on flooding was analysed to derive a flood susceptibility map. Second, potential TRM sites were identified to model sediment deposition in those areas. The potential impact of TRM on flooding was investigated by comparing flood susceptibility 'before and after' the implementation of TRM. To estimate flood susceptibility during the post-TRM scenario, geomorphological changes due to sedimentation in suitable sites were incorporated in the model.

2.1. Study area

The study focused on the south western coastal region of Bangladesh, containing 44 polders located in five coastal districts: Bagerhat, Jessore, Khulna, Pirojpur, and Satkhira (Figure 1 (a)). Approximately 5.3 million people live in this region (WorldPop, 2017), which includes areas from three physiographic regions of Bangladesh Ganges River floodplains, Ganges tidal floodplain, and old floodplain basins (Brammer, 2014). This low-lying deltaic region has a mean elevation of 3.5 m and is heavily intersected by tidal rivers. The Bangladesh Sundarban mangrove forest is located in the south of the study area.

Embankments were built in the study area from the 1960s to 1980s to protect about 5187 km^2 of land (WARPO, 2018). The region is mainly characterized by aquaculture lands and rural settlements (Abdullah et al., 2019). Although the region is prone to three types of flooding — pluvial, fluvio-tidal, and surge flood — pluvial flooding is the most frequent form of flooding (Adnan et al., 2019b). Frequent pluvial flooding (locally also referred to as 'waterlogging') in the region has decreased agricultural production and may have contributed to out-migration (Wilson et al., 2017). The region receives maximum precipitation during the monsoon months particularly from June to September, generating excess runoff. Inadequate drainage, due to deteriorating drainage channels and unreliable operation of sluice gates, contributes to frequent inundation in the low-lying 'beels'(Adnan et al., 2019b; Talchabhadel et al., 2018). The current study hypothesized that a loss in land elevation due to land subsidence contributed to a change in different geomorphological conditions determining the probability that an area will be flooded. Restoring sedimentation through TRM will promote a change in those flood conditioning factors, which will reduce the likelihood of flooding in the embanked region.

2.2. Flood inventory mapping

A flood inventory map of the study area was derived, analysing flood observation data obtained from remote-sensing imagery. Adnan et al. (2019b) identified the extent of annual flood inundation in the south western embanked region from 1988 to 2012 and attributed each flood to pluvial, fluvio-tidal, and storm surge flood events. The raster maps of binary (flood and non-flood) flood inundation maps of those 25 years were collected and overlaid in GIS to estimate the number of times (frequency) that different cells within the study area were inundated. Cells that remained flood-free were also identified (Figure S9 (a), supplementary document). The resultant flood inventory map was used to generate random flood and non-flood points for flood susceptibility modelling (Tehrany et al., 2019a). Applying a stratified random sampling method in GIS, we generated a vector layer of 1000 points where flood and non-flood locations were 586 and 414, respectively. The ratio of flood and non-flood locations was determined based on the proportion of the total area either affected or remained flood free during historical flooding, respectively. About 58.6% of the total area was inundated at least once during the floods from 1988 to 2012. The sample locations were split into two groups; 70% of samples (training data) were used to develop the flood susceptibility model and remaining 30% data (test data) were employed for validating the model (Table S2, supplementary document).

2.3. Deriving flood conditioning factors

The accuracy of hazard susceptibility map depends on the selection of hazard conditioning factors (Sabatakakis et al., 2013). Numerous studies have been conducted on flood hazard susceptibility mapping (Alam et al., 2017; Arabameri et al., 2019; Kabenge et al., 2017; Khosravi et al., 2016; Mojaddadi et al., 2017; Tehrany et al., 2014a; Tehrany et al., 2014b; Tehrany et al., 2017), with various combinations of flood conditioning factors being used. However, the selection of factors should be

based on the knowledge of morphological characteristics of the region under study (Tehrany et al., 2019a). Based on the knowledge obtained from the literature, initially 14 flood conditioning factors were selected under five broad categories: topographic, anthropogenic, geological, hydrological, and locational factors. Raster layers of the 14 flood conditioning factors were generated at 30m spatial resolution. Data used to produce those layers are listed in Table S1 of the supplementary document.

Topographic factors included aspect, elevation, slope, curvature, and land subsidence (Figure S1, supplementary document). Raster layers of the slope, aspect, and curvature were derived from the Advanced Land Observing Satellite (ALOS) Digital Elevation Model (DEM) (JAXA, 2015) in ArcGIS. Aspect denotes the direction of slope (Zevenbergen and Thorne, 1987), indicating the extent of precipitation and sunshine that an area would receive (Tehrany et al., 2017), which affects the water balance of an area (Singh et al., 2004). Together, elevation and slope influence the occurrence of flooding, as areas with a lower elevation and slope are more susceptible to flooding (Kabenge et al., 2017; Khosravi et al., 2016; Tehrany et al., 2014a; Tehrany et al., 2017). In relation to curvature, surfaces with flat or concave characteristics are more prone to inundation (Tehrany et al., 2017). This study assumes the land subsidence rate as a linear estimate (Brown and Nicholls, 2015). A layer of annual land subsidence rate was collected from Adnan et al. (2019b) where the natural neighbour interpolation method was applied in GIS to convert 205 point measurement of net subsidence (Brown and Nicholls, 2015) into a raster. Since the embanked region has been experiencing land subsidence from the beginning of polder construction in the 1960s, the annual land subsidence rate was multiplied by 52 (1960-2012) to obtain an estimate of total land subsidence since polder construction.

Four hydrological factors were selected: precipitation, flow accumulation, Stream Power Index (SPI), and Topographic Wetness Index (TWI) (Figure S2, supplementary document). To prepare the annual mean precipitation layer, 10-day gridded precipitation data from 1948-2012 was collected from the Bangladesh Meteorological Department (BMD). Flow accumulation, SPI, and TWI explain the characteristics of natural drainage. The flow accumulation layer was obtained from the DEM in GIS by deriving a continuous drainage network (Planchon and Darboux, 2002). Then, a flow direction raster was obtained, applying a single-direction flow algorithm (D8) where one cell routed into the next steepest of the eight neighbouring cells (Seibert and McGlynn, 2007). In the next step, a flow accumulation grid was generated, which indicates the accumulated sums of water flowing in the down-slope direction (Kabenge et al., 2017). SPI is a measure of the erosive power of surface runoff (Khosravi et al., 2016). SPI estimates the rate of sediment that would transfer to natural drainage channels. Areas with relatively high SPI values have a greater tendency to accumulate water (Bannari et al., 2017). TWI depicts the likelihood of a surface is wet. A higher TWI value of an area indicates a greater chance that the area will become wetter than the surrounding region (Bannari et al., 2017; Mojaddadi et al., 2017). SPI and TWI were derived using the following equations in GIS.

$$SPI = A_s \times \tan\beta \quad (1)$$

193

$$TWI = \ln\left(A_s/\beta\right) \quad (2)$$

194 where, A_s and β indicates the specific catchment area (m^2/m) and slope gradient respectively (Khosravi
195 et al., 2016; Regmi et al., 2010; Tehrany et al., 2014b).

196 Land use affects the rate of evapotranspiration and terrain infiltration, which are essential indicators
197 determining the extent and speed of runoff (Kabenge et al., 2017; Tehrany et al., 2019b; Thornthwaite
198 and Mather, 1957). Land use data that was collected for this research included thirteen classes (Figure
199 S3 (a), supplementary document). The geological factors included topsoil texture and soil permeability
200 (Figure S3 (b) and (c), supplementary document), which also explain the level of infiltration. For
201 instance, clay lowers the infiltration rate amplifying surface runoff (Bonacci et al., 2006). Generally,
202 the characteristics of soil and land use determine the water balance of an area (Thornthwaite and Mather,
203 1957). Polders are accompanied by drainage channels and sluice gates to impede saltwater intrusion in
204 the dry season, drain excessive rainwater, and allow fresh river water flow to polders in the wet season
205 for irrigation purposes (Adnan et al., 2019b). However, the construction of polders has reduced the tidal
206 prism, promoting sedimentation in tidal channels and infilled them (Wilson et al., 2017). Inadequate
207 drainage systems in the south western region increased inundation during historical pluvial flood events
208 (Adnan et al., 2019b). In the current study, data on the existing drainage network was collected from
209 Adnan et al. (2019b) who identified drainage channels from a high-resolution satellite image. Finally,
210 two layers were created showing the distance of a given area from adjacent drainage channels and rivers
211 in GIS, applying a Euclidean distance algorithm (Figure S3 (d) and (e), supplementary document).

212

213 **2.4. Flood susceptibility modelling**

214 A spatial regression model was developed for flood susceptibility mapping, applying an ensemble of
215 bivariate frequency ratio (FR) and multivariate logistic regression (LR) models. Recent studies have
216 followed different approaches to model flood susceptibility such as weight of evidence (Khosravi et al.,
217 2016; Tehrany et al., 2014b; Tehrany et al., 2017), decision tree (DT) (Tehrany et al., 2019a), support
218 vector machine (SVM) (Mojaddadi et al., 2017; Tehrany et al., 2019a; Tehrany et al., 2014b), FR
219 (Khosravi et al., 2016; Mojaddadi et al., 2017; Tehrany et al., 2017), analytical hierarchy process (AHP)
220 (Kabenge et al., 2017; Khosravi et al., 2016), LR (Pradhan, 2010; Tehrany et al., 2014a), and artificial
221 neural networks (ANNs) (Kia et al., 2012). An ensemble of FR and LR models was applied for the
222 following reasons: i) model development is less complex compared to different machine learning
223 techniques, such as ANN, DT, and SVM (Tehrany et al., 2019b); ii) the results of FR model are easy to
224 comprehend (Khosravi et al., 2016); iii) using an ensemble of two models reduces variance-error and

improves prediction accuracy (Althuwaynee et al., 2014); iv) it could potentially eliminate individual bias that the expert opinion-based AHP method is likely to produce, as AHP is based on pair-wise comparisons by experts (Althuwaynee et al., 2014; Tehrany et al., 2014a); v) LR can perform regression with independent variables with continuous and/or discrete type data (Althuwaynee et al., 2014); vi) LR can estimate the probability of occurrence of dependent variables (Bubeck et al., 2013).

2.4.1. Multi-collinearity diagnosis and optimizing flood conditioning factors

The selected flood conditioning factors could be subject to multi-collinearity, therefore, variance inflation factors (VIF) (Midi et al., 2010) of 14 selected flood condition factors were estimated using R (Fox et al., 2018), to eliminate the factors susceptible to multi-collinearity. VIF determines the degree of variance, indicating whether coefficients are inflated by multicollinearity. VIF of a variable exceeding 2.5 creates a concern for the model, while a value ≥ 10 indicates the presence of multicollinearity (Midi et al., 2010). Twelve flood conditioning factors with a VIF value ≤ 2.5 (Bai et al., 2011) were selected for modelling flood susceptibility (Table S3, supplementary document).

2.4.2. Frequency ratio (FR) model

The FR model aimed to measure the influence of each class in different flood conditioning factors on flood occurrence. A FR value greater or less than 1 indicates a strong or weak correlation of a factor class with the occurrence of flooding, respectively (Khosravi et al., 2016). For a flood conditioning factor, the FR was estimated using the following equation (Khosravi et al., 2016).

$$FR = \left[N_{pix}(SX_i) \Big/ \sum_{i=1}^{n} N_{pix}(SX_i) \right] \Big/ \left[N_{pix}(X_i) \Big/ \sum_{i=1}^{n} N_{pix}(X_i) \right] \quad (3)$$

where $N_{pix}(SX_i)$ denotes the number of training flood pixels within i^{th} class of independent variable X, $N_{pix}(X_i)$ is the total number of pixels within i^{th} class of independent variable X, and n is the total number of classes under variable X.

2.4.3. Logistic regression (LR) model

The statistical approach of flood susceptibility modelling assumes that the potential (probability of occurrence) of future flooding areas will be comparable to the frequency and extent of historical floods (Pradhan, 2010). The LR model incorporated 700 training flood observation data (flood and non-flood) as a dependent variable and 12 flood conditioning factors as independent variables. A weight to each cell in different flood conditioning factors was provided according to estimated FR, before incorporating them into the LR model (Althuwaynee et al., 2014; Tehrany et al., 2014a). The training flood observation data was used to extract the value of FR of 12 flood conditioning factors in GIS. Then regression coefficients and p-statistics of each variable as well as the coefficient of determinants (R^2)

of the model were estimated using the 'mlogit' package in R (Croissant and Croissant, 2018). The obtained regression coefficients were incorporated in equation (4) (Tehrany et al., 2014a) in GIS to derive the probability (p) of flood occurrence in the study area.

$$p = 1/(1 + e^{-z}) \quad (4)$$

where p is the probability of an event occurring. In the present situation, p is the estimated annual probability of flooding, indicating the likelihood of a cell being inundated annually, for a similar set of flood conditioning factors explicating inundated areas during the historical events; z is the linear combination of independent variables, which was estimated using the following equation.

$$z = b_0 + b_1x_1 + b_2x_2 + \cdots + b_nx_n \quad (5)$$

where b_0 is the model intercept, b_i (i = 1, 2, ..., n) indicates the regression coefficients of independent variables, and x_i (i = 1, 2, ..., n) represents the FR of n number of independent variables (Table 2). Obtained flood probability index map was categorized into five equal classes, representing different categories of flood susceptible zones. Besides, a cut-off flood probability value was optimised so that areas with flood probability above the cut-off value were classified as flood susceptible zones, and vice versa. The method used to optimize cut-off flood probability value is explained in Section 2.4.4.

2.4.4. Sensitivity analysis and model validation

The flood susceptibility model validation was performed using a well-known method called receiver operating characteristic (ROC) curve and subsequent area under the curve (AUC) (Althuwaynee et al., 2014; Arabameri et al., 2019; Khosravi et al., 2016; Tehrany et al., 2014a). ROC values express the ability of the model to correctly separate positive and negative observations in the validation samples (Arabameri et al., 2019). To develop this plot, the estimated annual flood probability values of all cells were sorted in descending order. Then the ordered flood probability index map was classified into 100 categories, with cumulative 1% (0.01) break. The resultant 100 categories of the probability index were plotted on the x-axis, which represents false-positive rates of annual flood probability. Then observed flood points were overlaid on the flood probability index map. The cumulative relative frequency of observed flood points (true positive rate) was plotted against each category of false-positive rate (Tehrany et al., 2019b).

The AUC is a global accuracy statistic, where the thresholds range from 0 (random prediction) to 1 (perfect prediction): Excellent (0.9–1), very good (0.8–0.9), good (0.7–0.8), moderate (0.6–0.7) and weak (<0.6) (Arabameri et al., 2019). AUC values estimated by using training and test data indicate the success and prediction accuracy of the model, respectively (Tehrany et al., 2019b). Moreover, observed relative flood frequency in each test flood location was plotted against corresponding modelled annual flood probability value and a third-degree polynomial regression model was established.

The values of various statistical indices such as overall accuracy, specificity, sensitivity, positive predictive value, negative predictive value (Tehrany et al., 2019b), and kappa statistic (McHugh, 2012) were estimated to measure the comparative performance of each model. Thus, modelled flood probability index values of all observed flood points (training and test) were binarized, optimizing a cut-off flood probability value using the 'OptimalCutpoints' package in R, which is "the optimal point on the ROC curve closest to the point (0, 1)" (López-Ratón et al., 2014).

2.5. Analysing the impact of TRM on flooding

2.5.1. Simulating sediment deposition in selected TRM sites

To model sediment deposition during the operation of TRM, suitable 'beels' were identified. 'Beels' were delineated using a DEM-based flood routing model (Diaz-Nieto et al., 2011), established for the south western embanked region by Adnan et al. (2019b). A total of 234 'beels' were identified within the embanked region, with sizes ranging from 0.74km^2 to 48.53km^2 (Figure 5 (a)). A GIS-based suitability analysis was performed to select TRM sites. First, indicators to perform suitability analysis were selected. Whilst limited information is available on indicators to select TRM sites, Masud et al. (2018) proposed a Sustainability Index of TRM (SITRM), conceptualizing the spatial and temporal impact of TRM based on a characterisation of the tidal river, environment, resilience, floodplain ecosystem, human health, and community. To identify suitable TRM sites, five indicators were selected: i) tidal prism; ii) river salinity; iii) flood prone areas; iv) crop production; and v) size of the 'beel'. These indicators are associated with the tidal river, environment, resilience, and floodplain ecosystem components of SITRM. The suitability analysis did not include indicators related to human health and community, due to unavailability of required spatial data for the entire study area.

The inter-tidal volume or tidal prism (P) explains the availability of tidal flow required to implement TRM. A higher P indicates an adequate tidal flow for TRM, given that water carries the required amount of sediment (Talchabhadel et al., 2018). The study area is comprised of lands from 46 river sub-basins and P was approximated in individual sub-basin using the following equation (Lakhan, 2003):

$$P = HA \tag{6}$$

where H is the tidal range and A is the surface area of each sub-basin. This is an approximation in basins where the inter-tidal area is significant relative to the overall surface area, but as the bathymetric form through the delta is rather similar, we do not expect this approximation to bias the results. Sub-basins were generated in GIS incorporating river outlet location data collected from BWDB, who also provided daily tidal water level data for each outlet. The difference between the mean water level in each outlet during the high and low tide is the tidal range.

Salinity is an important indicator of floodplain ecosystems. TRM operation allows river water to enter a tidal plain twice a day. A high concentration of salinity in tidal river water will cause an increase in

soil salinity, making land unsuitable for crop production (Masud et al., 2018). Therefore, the level of river salinity is inversely correlated with the suitability of a site to operate TRM. Monthly observed river salinity data in each outlet of river sub-basins was collected from the BWDB, which was averaged across the year, where salinity level ranged from 0.23dS/cm to 12.39dS/cm (Figure S9 (b), supplementary document). Since TRM primarily intends to minimize flooding problems, 'beels' that were frequently affected by flooding are more suitable for TRM. Hence, mean flood frequency in each 'beel' was estimated from the developed flood inventory map (Figure S9 (a), supplementary document). As, TRM primarily aims to increase crop production in flood-prone areas (Gain and Schwab, 2012), hence 'beels' with land used for agriculture are the most suitable TRM sites. Besides, relatively smaller 'beels' are more suitable for TRM implementation, which makes stakeholders engagement less complex (Masud et al., 2018).

A rank (y) was assigned to each 'beel' according to the level of suitability in a 1 (very low) to 5 (very high) scale, in relation to the value of each suitability parameter (x). Ranks were estimated applying a linear interpolation technique proposed by Davis (2002). If the value of a parameter is positively correlated with the level of suitability for a TRM site, then Equation 7 was used, otherwise, Equation 8 was applied (Adnan et al., 2019a). For land use data, a dummy code was provided to each land use class, based on subjective judgement (Abdullah et al., 2018). Three main categories of land use such as agriculture, mixed agriculture and aquaculture, and aquaculture were given codes of 3, 2, and 1, respectively.

$$If\ y\ \propto x, \qquad y_n' = \frac{(y_2 - y_1)(x_n' - x_{min})}{(x_{max} - x_{min})} + y_1 \tag{7}$$

$$If\ y\ \propto \frac{1}{x}, \qquad y_n' = \frac{(y_2 - y_1)(x_n' - x_{max})}{(x_{min} - x_{max})} + y_1 \tag{8}$$

where y_n' is the suitability rank of a parameter for the nth 'beel' (n = 1, 2, 3, …., 234); the maximum rank $y_2 = 5$; minimum rank $y_1 = 1$; x_n' is the value of a parameter for the nth 'beel'; x_{max} is the maximum value of a parameter among all 'beels', and x_{min} is the minimum value of a parameter among all 'beels'.

Simulated sediment deposition data were collected from Talchabhadel et al. (2018) for five 'beels' located in Polder 24 (Figure 1 (c)). Talchabhadel et al. (2018) simulated sediment deposition in TRM sites based on a two-dimensional (2D) numerical model, established through laboratory flume experiments to understand the mechanism of sediment transportation and deposition. During the experiment, a constant discharge of 5.1 l/s as upstream river flow and 2.8 l/s as downstream tidal flow were provided. To represent high and low tidal flow, the adjustable gate was used. The gate was kept closed for 2 minutes to represent high tide, when the downstream flow from water pump was supplied

along with dry sediment, of mean diameter equal to 94 μm and density 2.65 g/cc, from a sediment feeder. Then, the gate was opened for the next 2 minutes, when the downstream supply of water and sediment were stopped, representing a low tide. Thus, a total of 8 minutes of experiments were performed to represent two complete tidal cycles in a day, as is the case in the coastal region of Bangladesh. The study assessed the optimum size of the link canals and the importance of constructing cofferdams in the river upstream of the opening for effective sediment deposition around the attached tidal basin. To make the study less complicated, the experimental setup involved a straight river and tidal basin attached in a perpendicular alignment. Photogrammetric techniques were applied to measure the deposited sediment along with a laser displacement sensor (Figure S4-S7, supplementary document).

The 2D numerical model was developed based on the shallow water flow equations and suspended sediment transport. The model was applied to explore the efficacy of the land heightening of the tidal basin with changing discharges and opening sizes. The numerical models were tested in different scenarios and compared with experimental results. The model reproduced the water depth and velocity reasonably well (percentage bias = ± 5 % and coefficient of determination ≥ 0.7). Suspended sediment concentration (SSC) and the deposited sediment were also replicated in good agreement with experimentally measured data. The surface was divided by an unstructured mesh using the GID software developed by the International Center for Numerical Methods in Engineering (CIMNE) (https://www.gidhome.com). A DEM of 5m resolution was derived from the bathymetric data of March 2007 provided by the Institute of Water Modelling (IWM) Bangladesh. A Manning roughness coefficient of 0.025 was assigned to meshes covering the river system, channels, and connecting canals, whereas a Manning roughness coefficient of 0.04 was provided in remaining areas. Simulated sediment deposition during six months of TRM implementation in 'beel' Khukshia (*beel*-2, Figure 5 (b)) was further validated against observed sediment depth at various locations, collected through field-work in November 2012. Further details on the experimental setup, model development can be found in Talchabhadel et al. (2017) and Talchabhadel et al. (2018).

River bathymetry and measured sediment concentration data are not available for the whole area under study. Therefore, based on the simulated sediment deposition in five 'beels', sediment deposition in remaining 'beels' was parameterised, developing an ordinary least square (OLS) regression in GIS. The OLS model included pixelwise height of the deposited sediment as dependent variable and factors explaining the deposition of sediment as independent variables. Five geomorphological variables were identified that explained the height of the deposited sediment in each pixel: i) land elevation (E_l); ii) distance from drainage (link canal) (D_d); iii) TWI; iv) slope (S_l); and v) curvature (C). Figure S1-Figure S3 in the supplementary document show these variables. The estimated intercept and regression coefficients were used to form the Equation 9, which was applied to simulate sediment deposition in remaining suitable 'beels'.

$$Sediment\ deposition\ (m) = 1.73 - 0.13E_l - 0.13D_d - 0.04\,TWI - 0.03S_l + 0.04C \quad (9)$$

Validation of the developed OLS regression model was performed plotting the parameterized pixelwise sediment height in five 'beels' against the obtained modelled sediment height and estimating the R^2 value of 0.88 (Figure S8, supplementary document).

2.5.2. Estimating the impact of TRM on flooding

The change in land elevation and flood susceptibility for pre- and post-TRM implementation scenarios was compared. TRM has already been implemented in five 'beels' within Polder 24 (ADB, 2007), where simulation of sediment deposition was performed. A 50m resolution DEM was collected from IWM, which was developed from a toposheet map (1:20000) produced by Survey of Bangladesh (SoB) in 1990-1991, carrying out an aerial photography survey. The IWM and ALOS DEMs were used to estimate observed land elevation in pre-TRM and post-TRM scenarios in five 'beels', respectively. Because the TRM operations within these areas were interrupted before full sediment accumulation could occur, in practice land accretion was much lower than expected. In these cases, the sediment deposition was modelled for the remainder of the implementation period (1 to 5-year) to estimate the potential sediment accumulation during a 5-year implementation. Finally, the observed and modelled increase in land elevation were compared after the implementation of TRM.

A change in land elevation due to the implementation of TRM promoted changes in four other flood conditioning factors: aspect, slope, curvature, and Stream Power Index (SPI). Since TRM intended to alleviate land subsidence, hence the value of this factor was considered as zero for the post-TRM scenario. Parameterized sediment deposition was added to the existing ALOS DEM to develop DEM for the post-TRM scenario. Following the similar procedure explained in Section 2.4, flood susceptibility at post-TRM scenario was estimated.

3. Results and discussion

3.1. Delineation of flood susceptible zones

3.1.1. The outcome of the FR model

Table 1 summarizes the outcome of the FR model, showing the relationship between the flood conditioning factors and flooding. Areas with lower elevation and slope as well as curvature with flat and concave characteristics were prone to flooding. Regarding aspect, cells facing east, west, and northwest as well as flat areas were highly susceptible to flooding. A greater percentage of flood locations were found in areas where relatively higher level land subsidence occurred.

Table 1: Spatial relationship between flood locations and flood conditioning factors

Variables	Class	Frequency ratio (FR)	Variables	Class	Frequency ratio (FR)
Aspect	Flat (-1)	1.45	**Land uses**	Shrimp culture	0.93

Variables	Class	Frequency ratio (FR)	Variables	Class	Frequency ratio (FR)
	North (0-22.5)	0.84		Rice field	1.03
	Northeast (22.5-67.5)	0.92		Mixed rice field, shrimp, and other fish culture	3.52
	East (67.5-112.5)	1.00		Mangrove	0
	Southeast (112.5-157.5)	0.80		Shrimp and other fish culture	3.40
	South (157.5-202.5)	0.77		Other crop agriculture land	0.55
	Southwest (202.5-247.5)	0.95		Freshwater fish culture	1.41
	West (247.5-292.5)	1.02		River/Canal	1.26
	Northwest (292.5-337.5)	1.32		Settlement with Homestead Vegetation (Rural)	0.35
	North (337.5-360)	0.91		Settlement with Homestead Vegetation (Urban)	0.46
				Water Body	0
				Others	0
Elevation (m)	≤ 0	1.50	**Soil texture**	Silty clay and silty clay loam	1.78
	0 - 1	1.34		Clay	3.54
	1 - 2	1.29		Silty clay	0.88
	2 - 3	1.30		Silt loam and Silty clay	0.38
	3 - 4	0.98		Unclassified	0.96
	4 - 5	0.68		Silt loam	0.61
	5 - 7	0.25			
	7 - 9	0.15			
	> 9	0		Silty clay and clay	1.34
Slope (degree)	0 – 0.44	1.52		Silt loam and clay	1.02
	0.44 - 0.66	1.23		Silty clay loam and silty clay	0.86
	0.66 – 0.88	1.09		Silty clay loam and silt loam	0.43
	0.88 - 1.09	1.15		Silty clay loam	0
	1.09 - 1.32	0.84			
	1.32 - 1.98	1.09			
	1.98 - 2.64	0.78			
	2.64 - 3.73	0.69			
	3.73 – 56.01	0.38			
Curvature	Convex	0.98	**Soil permeability**	Moderate	0.58
	Flat	1.06		Mostly moderate	1.21
	Concave	1.00		Slow	1.25
Land subsidence (m)	< 0.12	0.32		Unclassified	0.96
	0.12 - 0.16	0.15		Mostly slow with some Moderate	0.39
	0.16 - 0.20	1.47		Mostly moderate with some slow	0.38
	0.20 - 0.23	1.95		Mostly slow	0.64
	0.23 - 0.25	1.17			
	0.25 - 0.26	1.15			
	0.26 - 0.265	0.83			
	0.265 - 0.27	0.69			
	> 0.27	1.31			
Precipitation (mm)	1593 - 1645	1.18	**Distance from drainage channels (m)**	0 - 90	0.93
	1646 - 1706	1.64		90 - 192.09	0.82
	1707 - 1766	1.06		192.09 - 308.87	1.17
	1767 - 1806	1.00		308.87 - 445.98	0.87

Variables	Class	Frequency ratio (FR)	Variables	Class	Frequency ratio (FR)
	1807 - 1863	1.20		445.98 - 607.45	1.10
	1864 - 1903	0.71		607.45 - 831.93	1.17
	1904 - 1948	1.10		831.93 - 1176.52	0.95
	1949 - 2178	1.04		1176.52 - 2012.01	0.92
	2179 - 2621	0.09		2012.01 - 13232.18	1.30
Stream power index (SPI)	-13.82 to -10.93	0.91	**Distance from rivers (m)**	0 - 180	0.89
	-10.93 to -10.19	1.05		180 - 450	0.95
	-10.19 to -7.02	0.40		450 - 780	0.84
	-7.02 to -3.48	1.30		780 - 1168.46	0.68
	-3.48 to -2.74	1.14		1168.46 - 1636.85	0.68
	-2.74 to -1.99	0.84		1636.85 - 2248.4	0.92
	-1.99 to -1.16	1.06		2248.4 - 3100.61	1.26
	-1.16 to 0.05	1.08		3100.61 - 4477.95	1.49
	0.05 to 10.01	1.32		4477.95 - 12559.4	1.18

Areas characterized by higher values of SPI contained a greater number of floods. Floods occurred primarily in areas that were used mostly for agricultural and aquaculture purposes, compared to settlement areas where a relatively lower number of flood locations were found. In relation to soil texture, four categories of soils contained most of the flood locations: 'silty clay and silty clay loam', 'clay', 'silty clay and clay', and 'silty clay loam and silty clay' type soil. Areas with 'moderate' or 'slow' permeable soils are prone to flooding. Besides, floods are more likely to occur in areas away from adjacent rivers, as water is difficult to drain from those areas.

3.1.2. The outcome of the LR model

Table 2 summarizes the outcome of the LR model. Among the 12 factors, six were statistically significant (p-value ≤ 0.05). The flood probability index map derived in this study is shown in Figure 2 (b). The optimization of flood probability values at observed flood locations yielded a cut-off (minimum threshold probability) value of 0.6. A major portion of the study area is susceptible to flooding, which was mostly inundated during different historical flood events (Figure 2 (a)). The annual probability of flooding in 48% of the studied area is ≥ 0.8, where observed mean relative flood frequency is 0.2. This result indicates that inundations occurred during four historical flood events, on average, as the maximum frequency of inundation was 20 in a total of 25 observation years (Figure S9 (a), Supplementary document).

Table 2: Logistic regression model to predict the occurrence or not occurrence of floods

Variables	Coefficient	Standard error	*p*-value
Intercept	-36.328	6.957	$1.778\ e^{-07}$ ***
Aspect (A_s)	0.023	0.008	0.003 **
Elevation (E_l)	0.045	0.004	$< 2.2e^{-16}$ ***
Slope (S_l)	-0.008	0.006	0.208
Curvature (C)	0.244	0.067	0.0002 ***
Land subsidence (L_s)	0.004	0.003	0.006 **
Precipitation (P)	0.008	0.005	0.087 ▪
SPI	0.003	0.007	0.614
Land use (L_u)	0.011	0.001	$8.221e^{-10}$ ***
Soil texture (S_t)	0.011	0.004	0.099 ▪
Soil permeability (S_p)	0.008	0.005	0.003 **

Distance from drainage channels (D_d)	0.011	0.010	0.372
Distance from rivers (R_d)	0.008	0.006	0.112

*R^2: 0.77; Significance codes: 0 '***' 0.001 '**' 0.01 '*' 0.05 '▪' 0.1 ' ' 1*

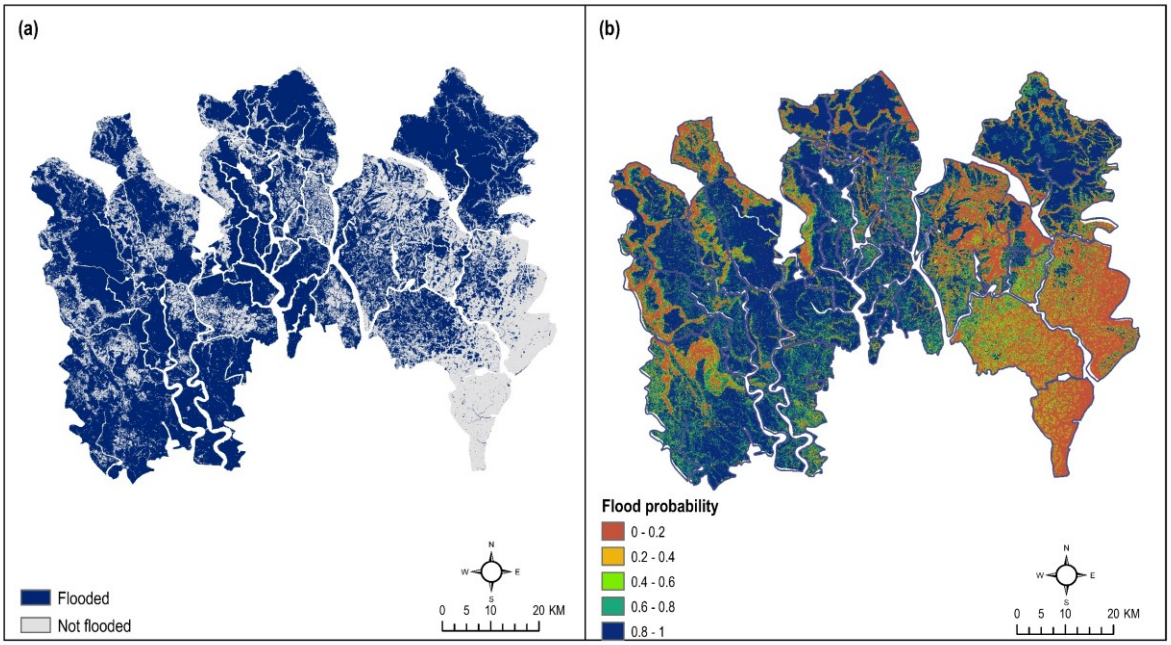

Figure 2: (a) Extent of inundation during floods from 1988-2012 (b) Annual flood probability index map

3.1.3. Model validation

The estimated AUC for test dataset was 0.86, which indicates a 'very good' prediction accuracy. In addition, the AUC of 0.90 for the training dataset implies an 'excellent' success rate of the model (Figure 3 (a)). Figure 3 (b) shows how the estimated flood probability increased with observed relative flood frequency. A third-degree polynomial equation was generated that explains the type of relationship between observed relative flood frequency and modelled flood probability. The general goodness of fit of this equation is verified by the estimated R^2 value of 0.97.

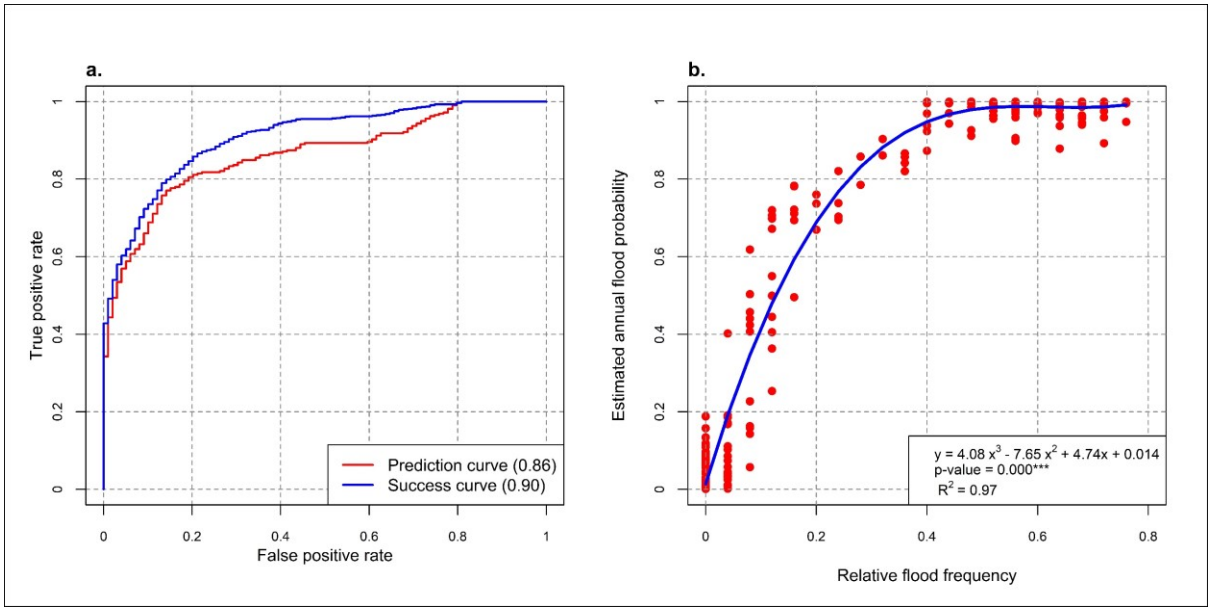

Figure 3: (a) ROC curve to validate flood probability map (b) Relative flood frequency and estimated annual flood probability of test flood observation points

Moreover, an overall accuracy of 93% explains the percentage agreement of pixels correctly classified. The Kappa coefficient of 0.85 indicates 'almost perfect' agreements between observed and modelled flood locations (Table 3).

Table 3: Validation of flood susceptibility model

Statistical index parameters	Values
True positive (correctly classified flood locations)	546
True negative (correctly classified non-flood locations)	381
False positive (incorrectly classified flood locations)	33
False negative (incorrectly classified non-flood locations)	40
Positive predictive value (PPV) (%)	95
Negative predictive value (NPV) (%)	90
Sensitivity (%)	93
Specificity (%)	92
Overall accuracy (%)	93
Kappa statistic	0.85

3.1.4. Characteristics of flood susceptible region

Since the average flood probability in most of the polders is greater than the minimum threshold flood probability, the major portion of the region is classified as being susceptible to flooding annually. More than 50% of the total area across 30 polders has an annual flood probability value ≥ 0.8 (Figure 4). The

major proportion of agricultural and aquaculture land use is located within flood susceptible zones (65% and 81%, respectively). More than 90% of the area under mixed agriculture and aquaculture land use is susceptible to flooding. A substantial proportion of people (44.5%) live in a relatively small proportion (22.8%) of settlement areas, which are susceptible to flooding (Table S4, supplementary document).

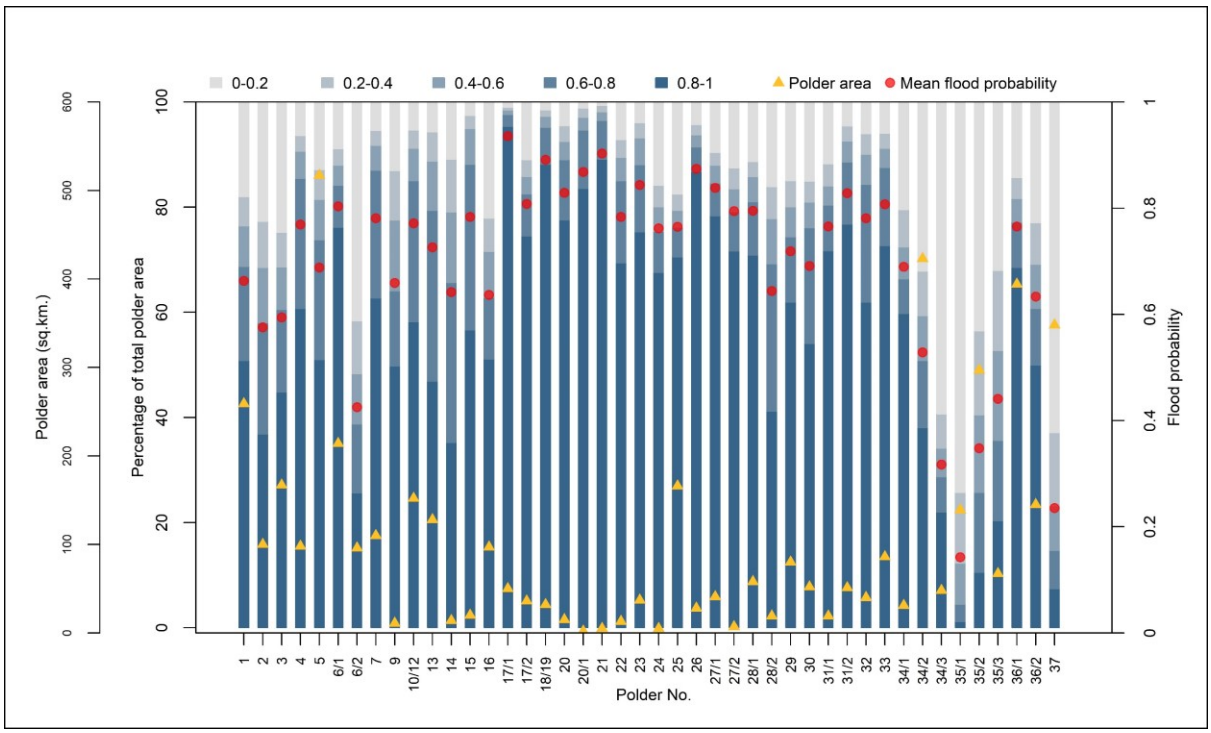

Figure 4: Ratio of flood susceptible lands in various polders

3.2. Impact of TRM in reducing flood susceptibility

3.2.1. Sediment deposition and restoring land elevation

The suitability analysis yielded 106 'beels' that are suitable (estimated suitability rank from 3 (moderate) to 5 (very high)) to operate TRM. Most of the polders in the northern segment of the study region are suitable, since these areas are highly prone to flooding and where most of the agricultural activities take place, and the salinity level in surrounding rivers is relatively lower (Figure 5 (a)). The result of the sediment transportation and deposition model indicated that continuous operation of TRM in sample 'beels' could reclaim a maximum of 1.4m land elevation in 5 years (Figure 5 (b)).

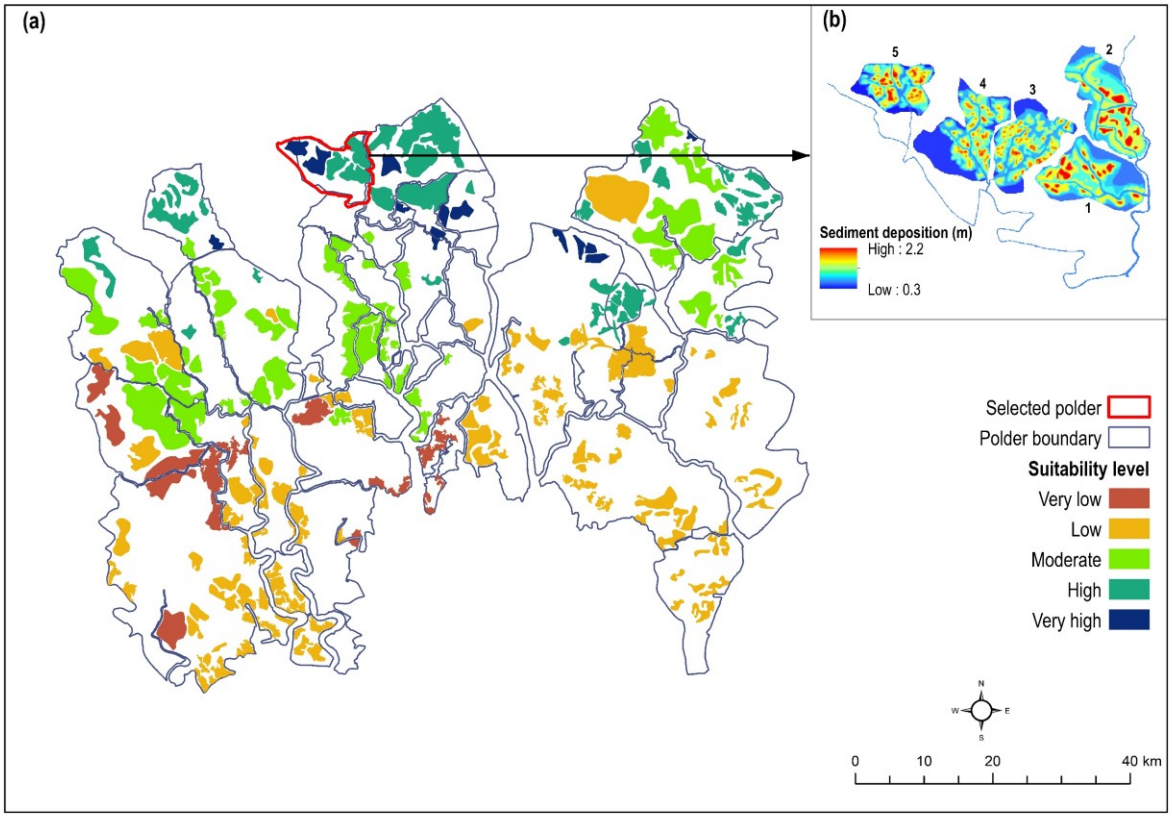

Figure 5: (a) Suitable 'beels' for TRM implementation; (b) sediment deposition in selected 'beels'

Figure 6 exhibits the extent to which TRM has been able to alter land elevation in five 'beels' in Polder 24. It also shows the land elevation that uninterrupted TRM might have recovered to in the five-year operation time. The mean elevation in all five 'beels' increased as a result of TRM (observed), implemented for various time steps. For instance, the length of TRM operation period in *beel*-1 (Beel Bhaina) was four years (1997-2001), whereas disruption in *beel*-2 ('Beel' Khukshia) caused an extended implementation period of six years (2006-2012). Results from the sediment transportation and deposition model indicated that an uninterrupted and planned implementation (e.g., construction of link canals, rotation of openings) of TRM might have led to a further increase in land elevation than which has been achieved. For instance, the three-year implementation of TRM in *beel*-1 might have recovered a similar depth of sediment that deposited in four years in practice. However, *beel*-2 is an example of an unsuccessful TRM, where interruptions occurred throughout the implementation period. The observed depth of sediment deposition in six years was similar to the estimated depth of sedimentation obtained after two years of TRM implementation. The analysis noted that TRM was the most successful in *beel*-5, as it yielded the highest depth of sediments.

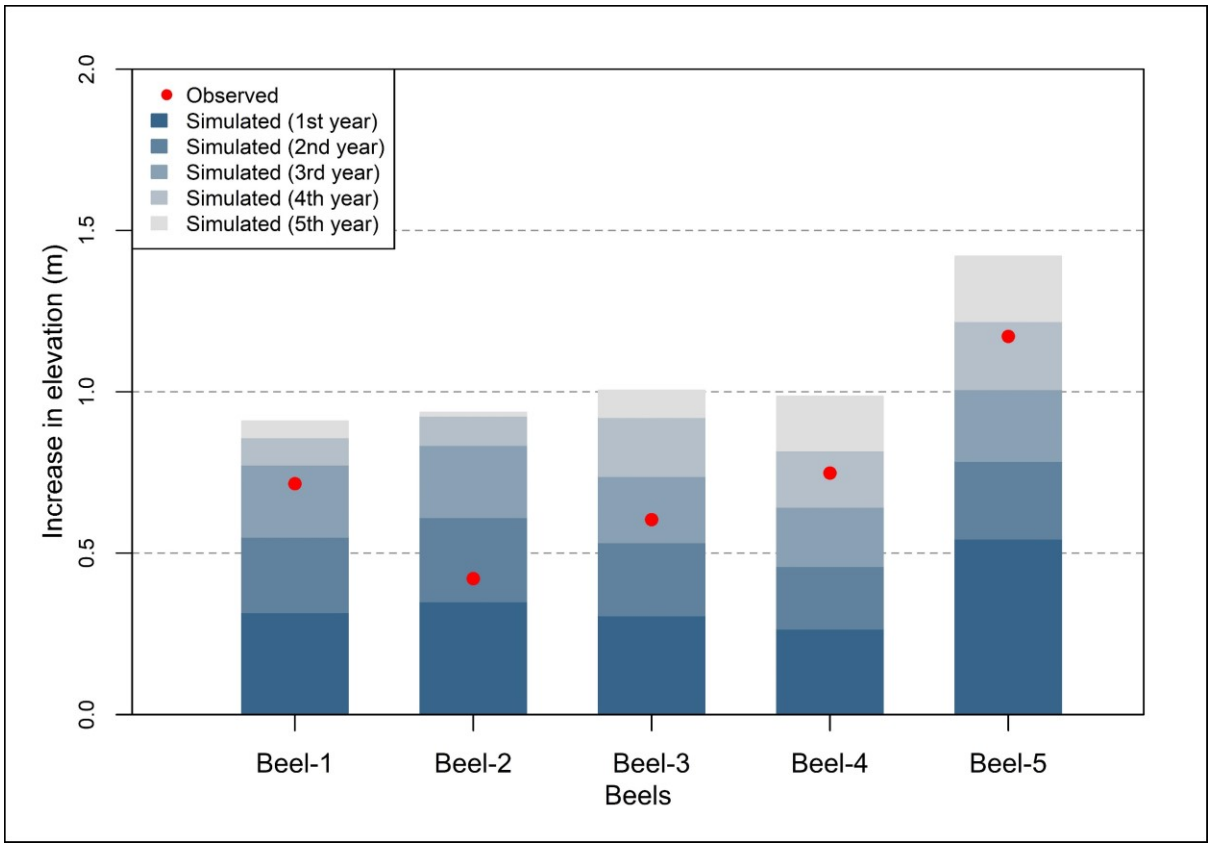

Figure 6: Change of land elevation in five selected 'beels' after implementing TRM

3.2.2. Flood susceptibility before and after TRM implementation

The application of TRM is predicted to reduce the annual probability of flooding from 0.86 (on average) to 0.57 (on average), in 106 suitable 'beels' located within 25 polders (Figure 7). A reduction of annual probability of flooding resulted from a change of various geomorphological flood-inducing factors. Along with increasing the surface elevation, the implementation of TRM could potentially improve the physical condition of natural drainage basin by reducing the value of SPI which reduces the erosion potential of the surface. Besides, changes in surface curvature would decelerate surface flow. All these changes result in a reduced annual probability of flooding in the TRM sites.

The implementation of TRM reduced flood susceptibility across 'beels' in 13 polders, which were susceptible to flooding before. In general, flood susceptibility in 35% of areas of the selected 'beels' reduced due to TRM. However, the impact of TRM varied across 'beels' in different polders. The maximum reduction in the annual probability of flooding was estimated in 'beels' located within Polder 20 and Polder 29 (Figure 7), where the probability of flooding reduced by 0.46 on average.

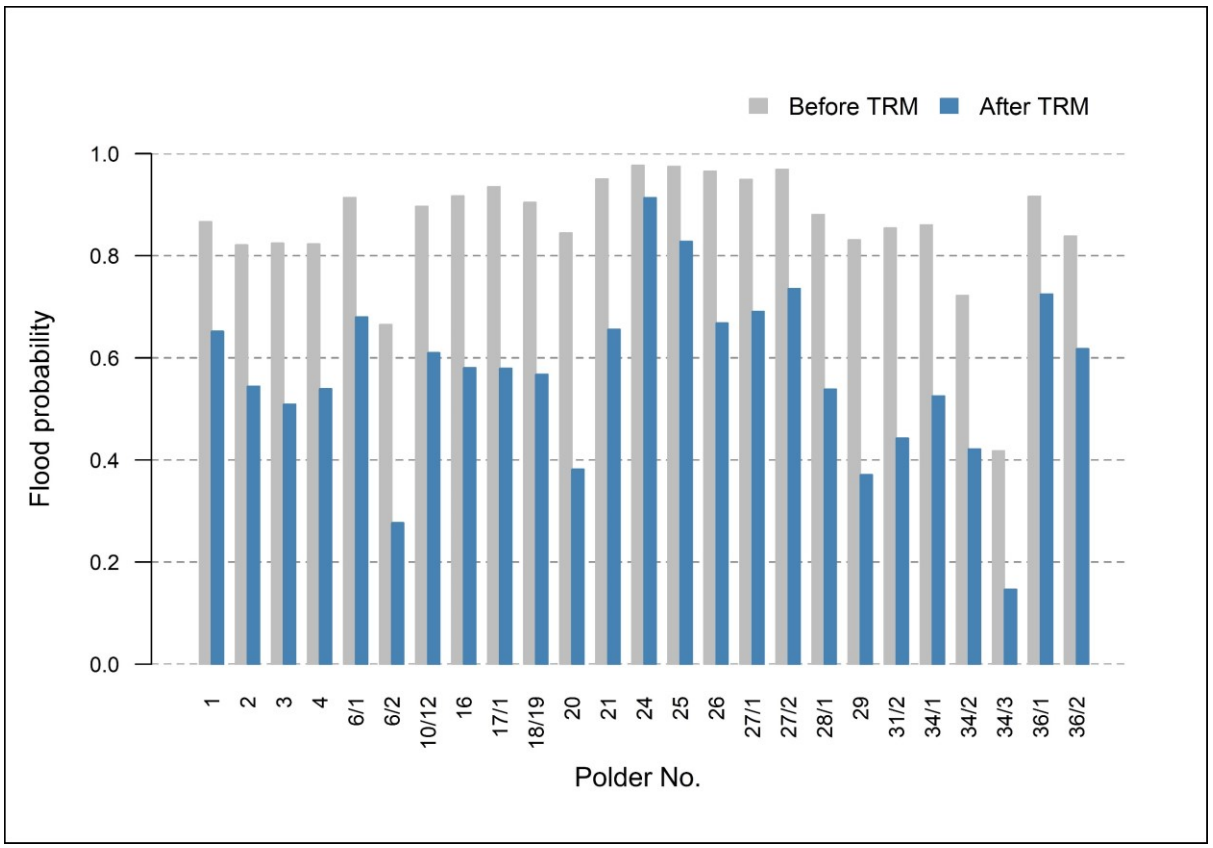

Figure 7: Annual probability of flooding in suitable 'beels' in different polders before and after the implementation of TRM

4. Conclusion

TRM in the south western coastal region of Bangladesh was implemented to promote sedimentation in low-lying 'beels', creating an opportunity of increased agricultural production by reducing flooding. In practice, the success of TRM was hampered by interruptions during its operation, primarily caused by various implementation hurdles such as social unrest, conflict, and issues related to compensation. This study modelled the potential effectiveness of TRM in restoring land elevation and reducing flood susceptibility in the study area. A flood susceptibility model has been developed that successfully predicts flooding locations based on coordination of conditioning factors, the most influential being land elevation, aspect, curvature, land use, land subsidence, and soil permeability. The study identified 106 suitable 'beels' where flooding could potentially be alleviated by a change in land elevation that could, in turn, be achieved by sediment deposition during TRM implementation. Sediment deposition in identified 'beels' was parameterised based on simulated sediment data on five sample 'beels'. Flood susceptibility in those 'beels' was compared between pre- and post-TRM implementation scenarios.

The results indicated that floods in the south western embanked region primarily occurred in areas with common characteristics such as low elevation and slope, flat landscape-scale curvature, high land subsidence rates and SPI, and moderate to low soil permeability. The study also estimated that a major

530 portion of the total region is susceptible to flooding, being inundated during various historical flood
531 events. Agricultural and aquaculture activities mostly take place in these flood susceptible zones. Wider
532 implementation of TRM would result in increased land elevation, which could alleviate land subsidence
533 and modify several geomorphological factors such as aspect, slope, curvature, and SPI. Such changes
534 in the surface could help to reduce the probability of flooding in a range of polders. The results described
535 here further indicate that an uninterrupted 5-year implementation of TRM might have resulted in a
536 greater increase in land elevation (in 'beels') than has actually been achieved in practice, due to
537 interruptions in implementation of several TRM projects.

538 Modelling sediment transportation in low-lying areas is a complex and data-intensive process. Scarcity
539 of data, including observed sedimentation, makes it difficult to model sediment deposition
540 hydrodynamically for the entire region. Accuracy of the flood susceptibility modelling results depends
541 on input parameters used, particular the DEM. The ALOS DEM is considered to be the most accurate
542 freely available DEM, which has a low root mean square error (1.78m) in vertical accuracy (Hasan et
543 al., 2020). To address the uncertainty related to DEM accuracy, topographical and hydrological
544 parameters were discretised into various quantile classes and incorporated to the flood susceptibility
545 model. Relevant discretised variables were also used to parameterise sediment deposition in suitable
546 'beels'.

547 This study attempted to assess the suitability of a site for TRM implementation mainly from the
548 perspective of the physical environment. Socio-economic and governance considerations have proved
549 to be critical to the successful implementation of TRM, but these have not been addressed in this study.
550 This study shows the extent to which an uninterrupted implementation of TRM could help to alleviate
551 flood susceptibility in the region. It further characterises polders according to the level of flood
552 susceptibility as well as suitability to implement TRM, which could be a useful guide for national
553 organizations like BWDB, who are responsible for managing water resources in polders.

554 **Acknowledgement**

555 This work is an output from the REACH programme (www.reachwater.org.uk) funded by UK Aid from
556 the UK Department for International Development (DFID) for the benefit of developing countries
557 (Aries Code 201880). However, the views expressed, and information contained in it are not necessarily
558 those of or endorsed by DFID, which can accept no responsibility for such views or information or any
559 reliance placed on them.

560 **5. References**

561 Abdullah AYM, Biswas RK, Chowdhury AI, Billah SM. Modeling soil salinity using direct and indirect
562 measurement techniques: A comparative analysis. Environmental Development 2018.
563 Abdullah AYM, Masrur A, Adnan MSG, Baky MAA, Hassan QK, Dewan A. Spatio-Temporal Patterns
564 of Land Use/Land Cover Change in the Heterogeneous Coastal Region of Bangladesh between
565 1990 and 2017. Remote Sensing 2019; 11: 790.

566 ADB. Bangladesh: Khulna-Jessore Drainage Rehabilitation Project - Project Performance Evaluation
567 Report. Asian Development Bank Bangladesh, 2007.
568 Adnan MSG, Dewan A, Zannat KE, Abdullah AYM. The use of watershed geomorphic data in flash
569 flood susceptibility zoning: a case study of the Karnaphuli and Sangu river basins of
570 Bangladesh. Natural Hazards 2019a; 99: 425–448.
571 Adnan MSG, Haque A, Hall JW. Have coastal embankments reduced flooding in Bangladesh? Science
572 of the Total Environment 2019b; 682: 405-416.
573 Alam MS, Sasaki N, Datta A. Waterlogging, crop damage and adaptation interventions in the coastal
574 region of Bangladesh: A perception analysis of local people. Environmental Development
575 2017; 23: 22-32.
576 Althuwaynee OF, Pradhan B, Park HJ, Lee JH. A novel ensemble bivariate statistical evidential belief
577 function with knowledge-based analytical hierarchy process and multivariate statistical logistic
578 regression for landslide susceptibility mapping. Catena 2014; 114: 21-36.
579 Amir MSII, Khan MSA. An Innovative Technique of Tidal River Sediment Management to Solve the
580 Waterlogging Problem in Southwestern Bangladesh. Coastal Management. Elsevier, 2019, pp.
581 165-199.
582 Arabameri A, Rezaei K, Cerdà A, Conoscenti C, Kalantari Z. A comparison of statistical methods and
583 multi-criteria decision making to map flood hazard susceptibility in Northern Iran. Science of
584 The Total Environment 2019; 660: 443-458.
585 Auerbach LW, Goodbred SL, Jr., Mondal DR, Wilson CA, Ahmed KR, Roy K, et al. Flood risk of
586 natural and embanked landscapes on the Ganges-Brahmaputra tidal delta plain. Nature Climate
587 Change 2015; 5: 153-157.
588 Awal M. Water logging in south-western coastal region of Bangladesh: local adaptation and policy
589 options. Science Postprint 2014; 1: e00038.
590 Bai S, Lü G, Wang J, Zhou P, Ding L. GIS-based rare events logistic regression for landslide-
591 susceptibility mapping of Lianyungang, China. Environmental Earth Sciences 2011; 62: 139-
592 149.
593 Bannari A, Ghadeer A, El-Battay A, Hameed NA, Rouai M. Detection of Areas Associated with Flash
594 Floods and Erosion Caused by Rainfall Storm Using Topographic Attributes, Hydrologic
595 Indices, and GIS. Springer International Publishing, Cham, 2017, pp. 155-174.
596 Bonacci O, Ljubenkov I, Roje-Bonacci T. Karst flash floods: an example from the Dinaric karst
597 (Croatia). Nat. Hazards Earth Syst. Sci. 2006; 6: 195-203.
598 Brammer H. Bangladesh's dynamic coastal regions and sea-level rise. Climate Risk Management 2014;
599 1: 51-62.
600 Brown S, Nicholls RJ. Subsidence and human influences in mega deltas: The case of the Ganges–
601 Brahmaputra–Meghna. Science of The Total Environment 2015; 527-528: 362-374.
602 Bubeck P, Botzen WJW, Kreibich H, Aerts JCJH. Detailed insights into the influence of flood-coping
603 appraisals on mitigation behaviour. Global Environmental Change 2013; 23: 1327-1338.
604 Choudhury NY, Paul A, Paul BK. Impact of costal embankment on the flash flood in Bangladesh: A
605 case study. Applied Geography 2004; 24: 241-258.
606 Croissant Y, Croissant MY. Package ‘mlogit’. 2018.
607 Davis J. Statistics and Data Analysis in Geology - 3rd Edition. John Wiley and Sons, USA, 2002.
608 Diaz-Nieto J, Lerner DN, Saul AJ, Blanksby J. GIS Water-Balance Approach to Support Surface Water
609 Flood-Risk Management. Journal of Hydrologic Engineering 2011; 17: 55-67.
610 Falconer R, Cobby D, Smyth P, Astle G, Dent J, Golding B. Pluvial flooding: new approaches in flood
611 warning, mapping and risk management. Journal of Flood Risk Management 2009; 2: 198-208.
612 Fox J, Weisberg S, Price B, Adler D, Bates D, Baud-Bovy G, et al. Package ‘car’. 2018.
613 Gain AK, Benson D, Rahman R, Datta DK, Rouillard JJ. Tidal river management in the south west
614 Ganges-Brahmaputra delta in Bangladesh: Moving towards a transdisciplinary approach?
615 Environmental Science and Policy 2017; 75: 111-120.
616 Gain AK, Schwab M. An assessment of water governance trends: the case of Bangladesh. Water Policy
617 2012; 14: 821-840.
618 Hasan MK, Kumar L, Gopalakrishnan T. Inundation modelling for Bangladeshi coasts using
619 downscaled and bias-corrected temperature. Climate Risk Management 2020; 27: 100207.

620 IPCC. Climate changes: The science of climate change, summary for policymakers and technical
621 summary of the working group 1 report. Intergovernmental Panel on Climate Change (IPCC),
622 Cambridge University Press, 1996.
623 Islam MA, Mitra D, Dewan A, Akhter SH. Coastal multi-hazard vulnerability assessment along the
624 Ganges deltaic coast of BangladesheA geospatial approach. Ocean & Coastal Management
625 2016; 127: 1-15.
626 JAXA. ALOS global digital surface model "ALOS world 3D-30m (AW3D30)". Japan Aerospace
627 Exploration Agency (JAXA), 2015.
628 Kabenge M, Elaru J, Wang H, Li F. Characterizing flood hazard risk in data-scarce areas, using a remote
629 sensing and GIS-based flood hazard index. Natural Hazards 2017; 89: 1369-1387.
630 Khosravi K, Nohani E, Maroufinia E, Pourghasemi HR. A GIS-based flood susceptibility assessment
631 and its mapping in Iran: a comparison between frequency ratio and weights-of-evidence
632 bivariate statistical models with multi-criteria decision-making technique. Natural Hazards
633 2016; 83: 947-987.
634 Kia MB, Pirasteh S, Pradhan B, Mahmud AR, Sulaiman WNA, Moradi A. An artificial neural network
635 model for flood simulation using GIS: Johor River Basin, Malaysia. Environmental Earth
636 Sciences 2012; 67: 251-264.
637 Lakhan VC. Advances in coastal modeling. Vol 67: Elsevier, 2003.
638 López-Ratón M, Rodríguez-Álvarez MX, Suarez CC, Sampedro F. OptimalCutpoints: an R package for
639 selecting optimal cutpoints in diagnostic tests. Journal of statistical software 2014; 61: 1-36.
640 Masud MMA, Moni NN, Azadi H, Van Passel S. Sustainability impacts of tidal river management:
641 Towards a conceptual framework. Ecological Indicators 2018; 85: 451-467.
642 McHugh ML. Interrater reliability: the kappa statistic. Biochemia Medica 2012; 22: 276-282.
643 Midi H, Sarkar SK, Rana S. Collinearity diagnostics of binary logistic regression model. Journal of
644 Interdisciplinary Mathematics 2010; 13: 253-267.
645 Mojaddadi H, Pradhan B, Nampak H, Ahmad N, Ghazali AHB. Ensemble machine-learning-based
646 geospatial approach for flood risk assessment using multi-sensor remote-sensing data and GIS.
647 Geomatics, Natural Hazards and Risk 2017; 8: 1080-1102.
648 Mutahara M, Warner JF, Wals AE, Khan MSA, Wester P. Social learning for adaptive delta
649 management: Tidal River Management in the Bangladesh Delta. International Journal of Water
650 Resources Development 2018; 34: 923-943.
651 Nowreen S, Jalal MR, Khan MSA. Historical analysis of rationalizing South West coastal polders of
652 Bangladesh. Water Policy 2014; 16: 264-279.
653 Planchon O, Darboux F. A fast, simple and versatile algorithm to fill the depressions of digital elevation
654 models. Catena 2002; 46: 159-176.
655 Pradhan B. Flood susceptible mapping and risk area delineation using logistic regression, GIS and
656 remote sensing. Journal of Spatial Hydrology 2010; 9.
657 Pradhan B, Oh HJ, Buchroithner M. Weights-of-evidence model applied to landslide susceptibility
658 mapping in a tropical hilly area. Geomatics, Natural Hazards and Risk 2010; 1: 199-223.
659 Regmi NR, Giardino JR, Vitek JD. Modeling susceptibility to landslides using the weight of evidence
660 approach: Western Colorado, USA. Geomorphology 2010; 115: 172-187.
661 Sabatakakis N, Koukis G, Vassiliades E, Lainas S. Landslide susceptibility zonation in Greece. Natural
662 Hazards 2013; 65: 523-543.
663 Seibert J, McGlynn BL. A new triangular multiple flow direction algorithm for computing upslope areas
664 from gridded digital elevation models. Water Resources Research 2007; 43.
665 Seijger C, Datta DK, Douven W, van Halsema G, Khan MF. Rethinking sediments, tidal rivers and
666 delta livelihoods: Tidal river management as a strategic innovation in Bangladesh. Water Policy
667 2019; 21: 108-126.
668 Singh RK, Hari Prasad V, Bhatt CM. Remote sensing and GIS approach for assessment of the water
669 balance of a watershed. Hydrological Sciences Journal 2004; 49: 131-142.
670 Talchabhadel R, Nakagawa H, Kawaike K. Sediment management in tidal river: A case study of East
671 Beel Khuksia, Bangladesh. E3S Web of Conferences. 40, 2018.
672 Talchabhadel R, Nakagawa H, Kawaike K, Hashimoto M, Sahboun N. Experimental investigation on
673 opening size of tidal basin management: a case study in southwestern Bangladesh. Journal of
674 Japanese Society of Civil Engineers, Ser B1 (Hydraulic Engineering) 2017; 73: I_781-I_786.

675 Tehrany MS, Jones S, Shabani F. Identifying the essential flood conditioning factors for flood prone
676 area mapping using machine learning techniques. CATENA 2019a; 175: 174-192.
677 Tehrany MS, Kumar L, Neamah Jebur M, Shabani F. Evaluating the application of the statistical index
678 method in flood susceptibility mapping and its comparison with frequency ratio and logistic
679 regression methods. Geomatics, Natural Hazards and Risk 2019b; 10: 79-101.
680 Tehrany MS, Lee MJ, Pradhan B, Jebur MN, Lee S. Flood susceptibility mapping using integrated
681 bivariate and multivariate statistical models. Environmental Earth Sciences 2014a; 72: 4001-
682 4015.
683 Tehrany MS, Pradhan B, Jebur MN. Flood susceptibility mapping using a novel ensemble weights-of-
684 evidence and support vector machine models in GIS. Journal of Hydrology 2014b; 512: 332-
685 343.
686 Tehrany MS, Shabani F, Neamah Jebur M, Hong H, Chen W, Xie X. GIS-based spatial prediction of
687 flood prone areas using standalone frequency ratio, logistic regression, weight of evidence and
688 their ensemble techniques. Geomatics, Natural Hazards and Risk 2017; 8: 1538-1561.
689 Thornthwaite CW, Mather JR. Instructions and tables for computing potential evapotranspiration and
690 the water balance. Drexel Institute of Technology, Centerton, NJ (EUA). Laboratory of
691 Climatology, 1957.
692 Van Staveren MF, Warner JF, Khan MSA. Bringing in the tides. From closing down to opening up delta
693 polders via Tidal River Management in the southwest delta of Bangladesh. Water Policy 2017;
694 19: 147-164.
695 Warner JF, van Staveren MF, van Tatenhove J. Cutting dikes, cutting ties? Reintroducing flood
696 dynamics in coastal polders in Bangladesh and the netherlands. International Journal of Disaster
697 Risk Reduction 2018; 32: 106-112.
698 WARPO. National Water Resources Database(NWRD). Water Resources Planning Organization
699 (WARPO), Bangladesh, 2018.
700 Wilson C, Goodbred S, Small C, Gilligan J, Sams S, Mallick B, et al. Widespread infilling of tidal
701 channels and navigable waterways in the human-modified tidal deltaplain of southwest
702 Bangladesh. Elementa-Science of the Anthropocene 2017; 5.
703 WorldPop. Bangladesh 100m Population, Version 2. University of Southampton. DOI:
704 10.5258/SOTON/WP00533 2017.
705 Zevenbergen LW, Thorne CR. Quantitative analysis of land surface topography. Earth surface processes
706 and landforms 1987; 12: 47-56.

707